Significant retrieval of lost evanescent power by tuning modes close-to-cutoff with a gel-coated taper

Huacai Chen,[1,2] Jianjun Ma,[2,*] Jiahua Chen,[2] and Wojtek J. Bock[2]

[1]*College of Optical and Electronic Technology, China Jiliang University, Xueyuan St. Xiasha Higher Education Zone, Hangzhou 310018, China*

[2]*Centre de Recherche en Photonique, Département d'Informatique et d'Ingénierie, Université du Québec en Outaouais, P. O. Box 1250, Hull Station, Gatineau, Québec J8X 3X7, Canada*

**Corresponding author: ma.jianjun@uqo.ca*

Received April 11, 2011; accepted April 22, 2011;
posted April 28, 2011 (Doc. ID 145787); published May 27, 2011

We report a fiber-optic evanescent-wave (EW) sensor capable of dramatically increasing the power collection level by capturing the EW power that is normally lost. The key element is a taper with a thin overlay that is completely separated from the sample by an arbitrary distance and thus operates remotely within the instrumentation system. A two-stage tuning of the close-to-cutoff modes occurring within this element is proposed to interpret the observed phenomenon.

OCIS codes: 060.2270, 060.2370, 300.6280.

Evanescent-wave (EW) based fiber-optic sensors are generally recognized as excellent tools for surface event analysis [1], but their use comes at the sacrifice of signal power strength. This is because the EW power is collected from the surface of the unclad fiber segment, and most of it is lost due to the significant difference between the normalized frequencies V, or to the V-number mismatch before it enters the clad segment [1–4].

To overcome this difficulty, a popular solution is to use a fiber taper or an optical overlay such as a sol-gel-derived film [1–7]. A diameter-reduced unclad segment [2] or a taper [3] diminishes the V-number mismatch by reducing the diameter of the unclad segment to match the mode populations of the clad and unclad segments. Consequently, a significant amount of EW power captured by the high-order modes of the unclad segment is allowed to enter the clad segment for detection. Alternatively, a sol-gel-derived overlay can act as an EW enhancer to boost the EW power by trapping analytes in a porous overlay and thus increasing the interaction between the EW fields and analytes [5–8]. But this approach raises critical issues regarding leaching, microstructural stability, diffusion response time, and susceptibility to interferents [6]. Solutions are often case-sensitive and very complicated, owing to the direct interaction between the sample and the signal enhancer—the sol-gel overlay. In fact, the traditional taper-based sensor designs rely on a similar interaction, taper-sample interaction, to enable the mechanism of EW power rise [1–3].

None of the above approaches, however, takes into account another equally strong EW power component that propagates away from the detector. In this Letter, we propose a simple element consisting of a taper and a thin refractive index (RI) gel overlay to efficiently access this normally lost EW power. Our design differs from many traditional sensor configurations in that this element serves as a signal enhancer but functions remotely, because within the instrumentation system it is completely separated from the sample by an arbitrary distance.

In Fig. 1, a 2-m-long fiber with a core diameter of 400 μm (BFL37-400, ThorLabs, Inc.) is adopted as the sensing fiber (s-fiber). One end of this fiber has a taper created via the heat-and-pull process. A fluorescence-capable sample, rhodamine 6G (R6G) water solution, is used for evaluating sensor performance. This sample encircles a mere 2-mm-wide cylindrical core located approximately 2 cm away from the taper. This sample can also be moved to any location along the unclad segment. The EW signal receiving end of the s-fiber, the R-end, is connected to the spectrometer, which records the EW signal power denoted by I_R. A second fiber of the same type, the excitation or e-fiber, illuminates the sample with the excitation laser light operating at 532 nm.

Depicted in Inset 1 of Fig. 1 is the R6G droplet shaped through surface tension by adjusting the relative positions of the s and e-fibers until the maximum fluorescent power is observed at the spectrometer. The excitation light path that maximizes the I_R is also shown. The advantages of such a sensing platform have been well summarized by us in previous papers [9,10]. Inset 2 in Fig. 1 illustrates the taper with three different surrounding media: air, thick RI gel, and a thin RI gel overlay. The thin overlay was formed by dipping the taper into a large gel block. The corresponding I_R for each of these cases is plotted in Fig. 2.

As shown in Fig. 1, the taper is located at a distance of 2 cm from the sample. It is crucial to notice that this taper

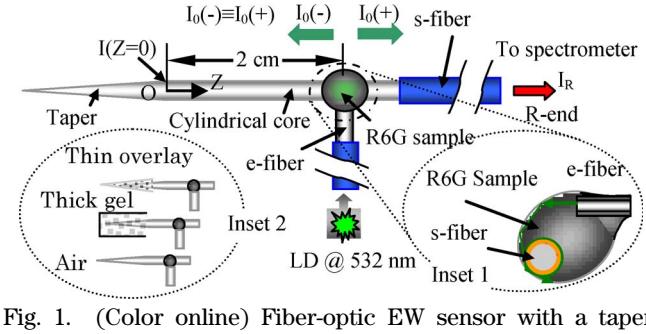

Fig. 1. (Color online) Fiber-optic EW sensor with a taper. (Inset 1) Arrangement of the fibers and the sample. (Inset 2) Tapers surrounded by air, or covered by thick or thin RI gel (part no. F1-0001, Fiber Instrument Sales, Inc.) overlay. The point of origin of the OZ axis starts at the taper–cylinder transition cross section.

as an enhancer functions substantially differently from a taper in a traditional system. In a traditional system, the taper must be completely immersed in the sample to enable its EW power enhancement mechanism. In contrast, there is no taper–sample contact here at all. Instead, the taper operates at the end of the *s*-fiber to remotely influence the EW power launched from the sample. This can be understood by noting the symmetrical architecture formed by the *s*-fiber, *e*-fiber, and the droplet in Fig. 1. The EW power emitted from the sample has two components that travel in opposite directions along the fiber, expressed by $I_0(+)$ and $I_0(-)$ and obeying the relation $I_0(+) \equiv I_0(-)$. Normally, only $I_0(+)$ will contribute to the I_R while $I_0(-)$ will be lost in a defect-free *s*-fiber and taper when both are surrounded by an infinite uniform medium such as air or thick RI gel, as indicated by the insets in Figs. 1 and 2. In this case, the *V*-number mismatch dominates the system performance and thus I_R has a very low level, as indicated by curves 1 and 2 in Fig. 2. Obviously, we can expect these two curves to be identical since they share the same degree of *V*-number mismatch. As shown in Fig. 2, we use I_{R0} to denote their power levels.

On the other hand, our investigation reveals that the tapered fiber element, when covered by a thin film of gel, has an unexpected ability to access $I_0(-)$, the power that is usually lost, and thus enhance the I_R level. Curve 3 of Fig. 2 shows that a tapered element with thin gel overlay enhances the I_R level 20 times more than a taper surrounded by air or thick gel.

For insight into the mechanism responsible for the observed phenomena in Fig. 2, let us refer to Fig. 1 again. The attenuation-free unclad cylindrical segment allows an arbitrary sample-taper separation, and thus

$$I(Z = 0) = I_0(-). \tag{1}$$

From our previous work [10] and other publications [1–3], both $I_0(+)$ and $I_0(-)$ arise primarily from the high-order guided modes and from the tunneling modes, with the latter operating just below cutoff and also being bound [11]. For the cylindrical segment from $Z = 0$ to the *R*-end in Fig. 1, the EW power strength along the fiber

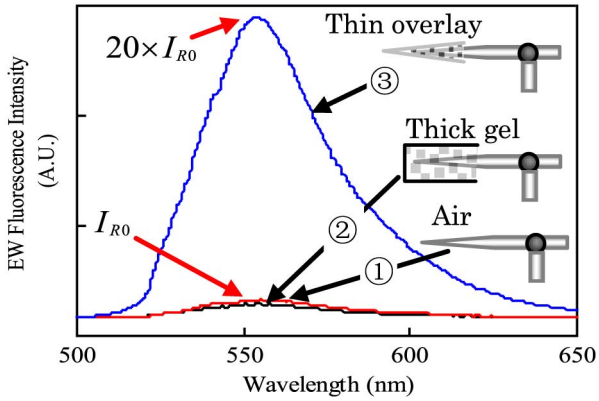

Fig. 2. (Color online) Recorded IR spectra illustrating the output powers for the three taper arrangments. I_{R0} is the level of the EW power I_R without the influence of the taper segment.

is restricted only by the RI of the cladding. Using the subscripts *h* and *t* to represent the high-order and tunneling modes, respectively, and lq to indicate the EW power permitted by the liquid-clad segment, we have

$$I_0(\pm) = {}^{\mathrm{lq}}I_{h,t}(\pm), \qquad I(Z = 0) = {}^{\mathrm{lq}}I_{h,t}(-). \tag{2}$$

A general expression of I_R can be written in the following form by including the contributions of both $I_0(+)$ and $I_0(-)$ components

$$I_R = {}^{\mathrm{cl}}I_{h,t}(+) + \eta_{h,t} \cdot {}^{\mathrm{lq}}I_{h,t}(-), \qquad \eta_{h,t} < 1, \tag{3}$$

where $\eta_{h,t}$ describes the combined capability of the high-order and tunneling modes to retrieve power from $I_0(-)$, the supposedly lost power, and to add it to I_R.

For the platforms associated with curves 1 and 2, the RIs of the core, cladding, and R6G liquid have values of 1.46, 1.41, and 1.33, respectively, yielding a significant *V*-number mismatch [2]. This means that approximately 60% of the high-order and tunneling modes in the liquid-clad fiber fails to propagate in the clad fiber [2,11], and thus

$${}^{\mathrm{lq}}I_{h,t}(+) \gg I_{R0}, \tag{4}$$

$$I_{R0} = {}^{\mathrm{cl}}I_{h,t}(+), \tag{5}$$

where the superscript cl indicates the power permitted by the clad segment. Equation (5) suggests that I_{R0} arises from the high-order and tunneling modes of the clad segment.

Recalling that the $I_0(-)$ component does not contribute to curves 1 and 2, we can write Eq. (3) as

$$I_R = {}^{\mathrm{cl}}I_{h,t}(+) = I_{R0}, \qquad \eta_{h,t} = 0. \tag{6}$$

When considering the platform associated with curve 3 in Fig. 2, Eq. (3) will be

$$I_R \approx \eta_{h,t} \cdot {}^{\mathrm{lq}}I_h(-) \gg I_{R0}. \tag{7}$$

Equations (6) and (7) further reveal that, while stemming from ${}^{\mathrm{lq}}I_{h,t}(+)$, the power propagating toward the detector, the level of I_{R0} is so low as to be negligible compared to $\eta_h \cdot {}^{\mathrm{lq}}I_{h,t}(-)$, the power traveling away from the detector and supposedly lost. Clearly, this astonishing phenomenon results from the fact that the taper covered by a thin film of gel is able to retrieve part of $I_0(-)$ and send it to the *R*-end for detection. Remarkably, the significant rise we recorded in I_R is achieved despite the presence of the *V*-number mismatch, indicating that the mechanism responsible is mode coupling (or tuning) occurring after the power $I(Z = 0)$ enters the taper–overlay element. It is this mode-tuning process that transfers a part of $I_0(-)$ to the modes permitted by the clad fiber segment, which effectively circumvents the obstacle of *V*-number mismatch.

The taper shown in Fig. 3(a) has an angle of 3.3° and a taper ratio (TR) of TR = 0.85, making it a weak mode converter [4]. The same taper appears in Fig. 3(b), in an image taken by a low-sensitivity CCD camera that shows the strong leak of $I_0(-)$ clearly tracing the outline

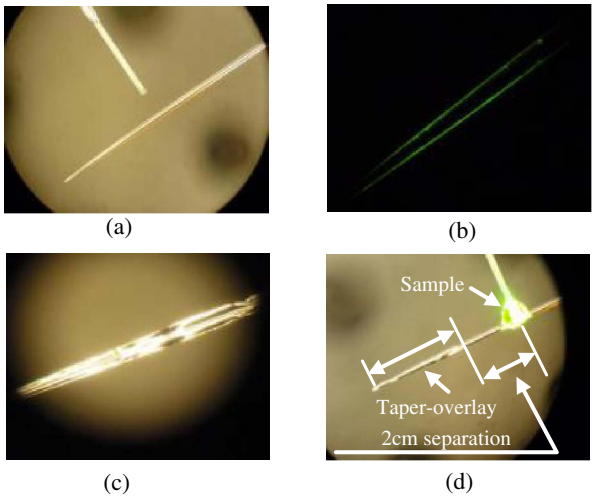

Fig. 3. (Color online) Photograph showing the characteristics of the platform. (a) Long taper; (b) taper profile traced by the leaked power $I_0(-)$; (c) appearance of the taper-overlay element; (d) platform in operation mode, showing that the EW power increase is triggered externally. Refer to the text for detail.

of the taper. These facts together suggest that the taper has converted the bound modes, described by Eq. (2), into leaky modes. For a weak mode converter, such conversion is only possible when the bound and leaky modes are neighboring modes. Obviously, the bound modes next to the leaky modes are those close-to-cutoff (CTC), including the few high-order modes near cutoff and a large number of tunneling modes. The power $I(Z=0)$ thus comes mainly from the CTC modes and Eq. (2) should be modified to

$$I(Z=0) \approx {}^{\mathrm{lq}}I_{\mathrm{ctc}}(-) = {}^{\mathrm{lq}}I_{\mathrm{h\_ctc}}(-) + {}^{\mathrm{lq}}I_t(-), \qquad (8)$$

where the subscript t, rather than t_ctc, appears in term ${}^{\mathrm{lq}}I_t(-)$, since by definition the tunneling modes operate just below cutoff.

Being extremely sensitive to any irregularities in the fiber, a CTC mode may be tuned to a leaky mode and vice versa, depending on the distribution of irregularities. The 20-fold increase of I_R in Fig. 2 is the result of this two-stage opposite mode tuning. In the first stage, a complete mode tuning from CTC to leaky is enabled by the fiber taper, the first irregularity. Upon encountering the second irregularity, the gel overlay, the mode launches into the second stage, which tunes some of these leaky modes into bound ones. Based on Eqs. (7) and (8), the strength of the I_R after this two-stage tuning may be expressed as

$$\begin{aligned} I_R &\approx \eta_{\mathrm{ctc}}\,{}^{\mathrm{lq}}I_{\mathrm{ctc}}(-) \\ &= \eta_{\mathrm{h\_ctc}}\,{}^{\mathrm{lq}}I_{\mathrm{h\_ctc}}(-) + \eta_t\,{}^{\mathrm{lq}}I_t(-), \qquad \eta_{\mathrm{ctc}}, \eta_{\mathrm{h\_ctc}}, \eta_t < 1, \end{aligned} \qquad (9)$$

where the coefficient η_{ctf}, η_{h_ctc}, or η_t describes the efficiency of this two-stage tuning from the CTC modes to those permitted by the clad segment. The tuning is strongly affected by the overlay geometry and the participating mode population. Under microscope with the 400-μm-core diameter as the reference, the thickness of the thin gel overlay in Fig. 3(c) is found to vary randomly around ~50 μm. This thin, transparent, and irregularly shaped overlay, together with the taper and the more than 4×10^5 tunneling modes plus high-order modes allowed by the 400-μm-core s-fiber [[11], Chap. 24], could enormously intensify the mode tuning across the entire overlay and the taper when the instrumentation system is in operation, as shown in Fig. 3(d). This could, in turn, considerably magnify η_{ctc} or η_{h_ctc} and η_t. In fact, our experiment shows that the 20-fold increase of I_R in Fig. 2 can be achieved rather easily even with a randomly formed overlay not subject to quality control. This fact implies that a small nonzero η_{ctc}, η_h, or η_t is probably sufficient for a significant rise of I_R, since $I_0(-)$, described by Eqs. (2) and (3), is strong enough to validate Eq. (7).

We are aware that by attaching a mirror to one end of the cylindrical fiber to replace the s-fiber in Fig. 1, one can also retrieve the lost $I_0(-)$. However, while this will double the I_R level of curves 1 and 2 in Fig. 2, it will not induce a 20-fold enhancement, since the mirror itself can not overcome the barrier of the V-number mismatch.

In conclusion, we have demonstrated that a simple fiber taper coated with a thin layer of RI gel can function as a highly efficient EW power enhancer by retrieving the otherwise lost $I_0(-)$ component. Remarkably, this enhancer operates at an arbitrary distance away from the sample, eliminating the problems stemming from physical contact between the sample and the EW power enhancer, for example, between the sample and the sol-gel mentioned earlier. Moreover, this signal increase is achieved without coping with the V-number mismatch and no strict overlay or taper quality controls is required. Yet, despite these merits, we will continue to optimize the gel thickness and the irregularities in combination to see the possibility to further increase I_R significantly.

The authors gratefully acknowledge support for this work from the Natural Sciences and Engineering Research Council of Canada, from the Canada Research Chairs Program, and from the Ministère de Développement Économique, Innovation et Exportation du Québec.

References

1. C. R. Taitt, G. P. Anderson, and F. S. Ligler, Biosens. Bioelectron. **20**, 2470 (2005).
2. G. P. Anderson, J. P. Golden, and F. S. Ligler, IEEE Trans. Biomed. Eng. **41**, 578 (1994).
3. J. P. Golden, G. P. Anderson, S. Y. Rabbany, and F. S. Ligler, IEEE Trans. Biomed. Eng. **41**, 585 (1994).
4. M. Ahmad and L. L. Hench, Biosens. Bioelectron. **20**, 1312 (2005).
5. B. D. MacCraith, V. Ruddy, C. Potter, B. O'Kelly, and J. F. McGilp, Electron. Lett. **27**, 1247 (1991).
6. B. D. MacCraith, C. McDonagh, A. K. McEvoy, T. Butler, G. O'Keeffe, and V. Murphy, J. Sol-Gel Sci. Technol. **8**, 1053 (1997).
7. B. D. MacCraith and C. McDonagh, J. Fluoresc. **12**, 333 (2002).
8. W. Cao and Y. Duan, Sens. Actuators B Chem. **119**, 363 (2006).
9. J. Ma and W. J. Bock, Opt. Lett. **32**, 8 (2007).
10. J. Ma, W. J. Bock, and A. Cusano, Opt. Express **17**, 7630 (2009).
11. A. W. Snyder and J. D. Love, *Optical Waveguide Theory* (Chapman and Hall Ltd., 1983).